International Journal of Science & Technology (PRAGYANAM)
Volume 1 • Issue 1 • January–December 2025
ISSN:

Absorption Enhancement in Silicon Solar Cell by Incorporation of Metal Nanoparticles

Mohd Amir[1], Mukesh Pratap Singh[2] & Iram Masood[3]

ABSTRACT

This study investigates the impact of strategically positioned metal nanoparticles (NPs) like Gold (Au), aluminum (Al), silver (Ag), and copper (Cu) on thin-film silicon (Si) to enhance optical absorption. The integration of NPs diminishes surface reflectance through forward scattering and near-field effects, thereby enhancing light coupling into the Si through the plasmonic properties of NPs. This dual enhancement in optical performance is achieved by optimising the radius and period of NPs. Subsequently, a comparative analysis is conducted among devices incorporating these NPs individually, revealing that Cu NPs yield the most significant absorption enhancement. A notable relative increase of 139.72% is observed in the current density (J_{SC}) with the utilisation of Cu NPs compared to the reference device, which lacks NPs. All simulations are executed using Lumerial finite-difference time-domain (FDTD) software.

Keywords: Thin Si Solar Cell, Metal Nanoparticles, Plasmonic, Light Trapping, FDTD

INTRODUCTION

Plasmons represent collective oscillations of free electrons within a material. These quasi-particles are similar to photons and phonons, arising from the quantization of plasma excitations [1], [2]. In recent years, plasmonic has emerged as a rapidly advancing field of research. This growth can be attributed to the continuous advancement in the fabrication and characterization methods of materials at nanoscale [3]–[5]. Additionally, various electromagnetic simulation techniques have been developed for understanding and harnessing plasmonic phenomena [6]–[8]. By adjusting the plasmonic properties, such as size and shape, of material at nanoscale, they find applications in various modern technologies, including photovoltaics (PV), plasmonic integrated circuits, plasmonic lasers, surface plasmon-enhanced LEDs, and bio-sensing [9], [10]. Plasmonic structures can be categorized into subgroups such as nanowires, nanorings, and nanoparticles, all of which exhibit unique optical characteristics due to their nanoscale dimensions. Consequently, the optical properties of materials at the interface of dielectric and metal nanostructures undergo significant changes, leading to modifications in the local dielectric environment [3]–[5], [11]–[13]. When exposed to sunlight, surface plasmon resonance (SPR) occurs near the metal-dielectric interface, resulting in a strong enhancement of the electromagnetic (EM) field at the interface. The plasmons are those SPR that are resulted due to the interaction of nanostructures with the light, where collective oscillation of free electrons take place under the influence of oscillating electric field. The plasmons are broadly classified into three major categories namely localised surface plasmon (LSP), bulk plasmon (BP), and surface plasmon polaritons (SSP) [1], [2], [14].

One of the major drawbacks of PV technology is its high price of power per unit watt, compared to the available traditional power generation technologies. The cost of the power generated by Si-based PV may be reduced significantly by lowering the amount of material (Si) consumption in the manufacturing of these cells i.e., by optimising their thickness, while keeping the light absorption within the adequate limits. The use of metal nanoparticles (NPs) in the thin Si-based PV have a high potential to boost up

[1] Department of Applied Sciences & Humanities, Jamia Millia Islamia, New Delhi, India. E-mail: mohd169066@st.jmi.ac.in
[2] Department of Applied Sciences & Humanities, Jamia Millia islamia, New Delhi, India. E-mail: mpsingh@jmi.ac.in
[3] Department of Applied Sciences & Humanities, Jamia Millia Islamia, New Delhi, India. E-mail: iram188891@st.jmi.ac.in

their absorption ability by the means of plasmonic properties of NPs [5], [15]. The incorporation of the NPs scatters the light to large angles into the absorbing material (Si in this case) which increases the path length of the light and hence the reflection losses are minimised. Subsequently, the plasmonic effect like LSP may further enhance the absorption within the Si leading to high generation rate within the active material (Si) [2], [5], [8], [15], [16]. The incorporation of NPs in Si PV provides a cost-effective solution of enhancing its performance and reducing the cost of power per unit watt. The metal nanoparticles such as Al, Ag, Au, and Cu are some most commonly used materials in the Si-based PV due to their exceptional optoelectrical properties [15], [17]. These NPs shows excellent scattering and/or light absorbing properties. It is mandatory to maximise the scattering effect while minimising absorption within the nanoparticles themselves, across the range of wavelengths of interest. This delicate balance is required for optimising the photon-to-electron conversion efficiency within the device. The effective light trapping using the NPs in the thin films have been demonstrated by the Atwater et al. [18]. Spinelli et al. has optimised NPs arrays through impedance matching with the Si substrate, resulting in a substantial enhancement of absorption across a broad range of frequencies of the incident light [19]. It has also been reported in the literature that the side-coated mental NPs shows an ability to maximise the light coupling into the Si nanowires that significantly enhance the absorption [20]. The absorption enhancement within the Si nanowires has also been resulted via incorporation of metal NPs specifically in the long-wavelength region of the light spectrum [21], [22]. A study on the effect of Au NPs deposited on the Si nanopillars and nanoholes has been conducted by the Pudasaini et al. [23]. Whereas Huang et al. has shown an efficient light trapping within the Si nanopillars, using Ag nanospheres on the top of Si nanopillars [24]. The literature also reveals that the path length reduces, on increasing the gap between the NPs and the absorbing medium, resulting in substantial reduction in the scattering effect of the NPs. Therefore, it is crucial to maintain an appropriate gap between these two components [25].

The further advancement of the technology requires an analysis of light harvesting properties of the combined structure, consisting different metal NPs such as Al, Ag, Au, and Cu. This critical examination of the different metal NPs may help the researchers and the industrialist to identify the most suitable metal NPs for the Si PV cells. In this work, we have performed a comparative numerical study to investigate the effect of various metal NPs (Al, Ag, Au, and Cu) on the absorption of Si PV cells. For the purpose we have designed four distinct devices (Device – A, B, C, D), comprising Al, Ag, Au, and Cu metal NPs, respectively, directly positioned on top of the Si substrate. To enhance the scattering and plasmonic effects leading to high absorption within the device, we have optimised the radius and the period of the metal NPs. A performance comparison is also made among all the devices at their respective optimised values of radius and the period.

SIMULATION DETAILS

This work utilises the Finite-Difference Time-Domain (FDTD) methods for executing all the simulation within the Lumerical program software. The program solves the Maxwell's electromagnetic (EM) wave equations described by the equations (1) to (4) in differential form.

$$\nabla.E = \rho / \varepsilon \quad ...(1)$$

$$\nabla.B = 0 \quad ...(2)$$

$$\nabla \times E = -\partial B / \partial t \quad ...(3)$$

$$\nabla \times H = J + \partial D / \partial t \quad ...(4)$$

where, electric filed is represented by E, magnetic flux is denoted by B, D is used for the displacement vector of electric filed, and H shows the magnetic field. While the ρ and J are the volume charge density and current density, respectively. In the context of a Cartesian coordinate system, the expansion of the curl equations described above results in a set of six scalar equations as given below:

$$\frac{\partial E_x}{\partial t} = \frac{1}{\varepsilon}\left(\frac{\partial H_z}{\partial y} - \frac{\partial H_y}{\partial z} - \sigma E_x\right) \quad ...(5)$$

$$\frac{\partial E_y}{\partial t} = \frac{1}{\varepsilon}\left(\frac{\partial H_x}{\partial z} - \frac{\partial H_z}{\partial x} - \sigma E_y\right) \quad ...(6)$$

$$\frac{\partial E_z}{\partial t} = \frac{1}{\varepsilon}\left(\frac{\partial H_y}{\partial x} - \frac{\partial H_x}{\partial y} - \sigma E_z\right) \quad ...(7)$$

$$\frac{\partial H_x}{\partial t} = -\frac{1}{\mu}\left(\frac{\partial E_z}{\partial y} - \frac{\partial E_y}{\partial z}\right) \quad ...(8)$$

$$\frac{\partial H_y}{\partial t} = -\frac{1}{\mu}\left(\frac{\partial E_x}{\partial z} - \frac{\partial E_z}{\partial x}\right) \quad ...(9)$$

$$\frac{\partial H_z}{\partial t} = -\frac{1}{\mu}\left(\frac{\partial E_y}{\partial x} - \frac{\partial E_x}{\partial y}\right) \quad ...(10)$$

Where σ is the conductivity and μ is the magnetic permeability. The equations (5) to (7) defines the temporal derivatives of electric field with respect to the spatial derivatives of the magnetic fields. In contrast, the subsequent three equations (8) to (10) describes the temporal derivatives of magnetic field with respect to the spatial derivatives of the magnetic fields. These scalar equations serve as the foundation for the FDTD method, which is used to simulate the interactions of EM waves with the materials in three-dimensional space. The Maxwell's curl equations are solved using Yee's algorithm by the program, which employs central difference numerical techniques for both spatial and temporal derivatives [26], [27]. The algorithm discretises the entire three-dimensional space into infinitely small cubic cells, known as Yee cells. This differs from the conventional method of separately calculating electric and magnetic fields by solving the wave equation. Within a single Yee cell, the normal to the faces of the cell represent the magnetic field vectors, while the edges of the cell define the electric field vectors [26], [27].

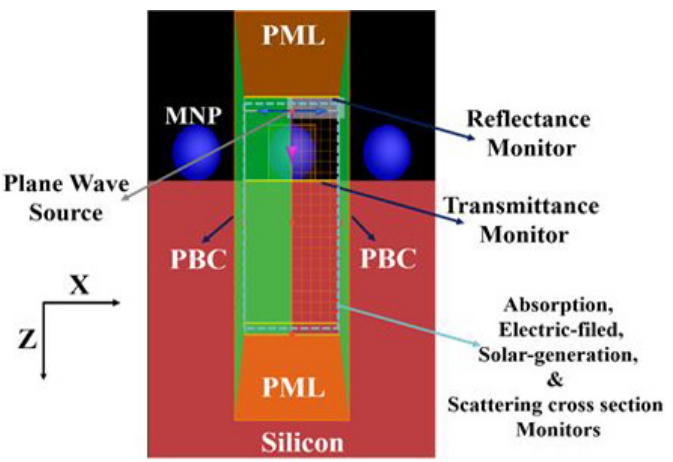

Fig. 1. A snapshot of FDTD simulation of the designed device

Fig. 1 provides a snapshot of the designed device, which includes spherical nanospheres (NSs) directly positioned on top of the Si substrate (1000 nm thick), with a specified radius (r) and period (p). The period is defined as the centre-to-centre distance between the two consecutive NSs. In FDTD the periodic boundary conditions (PBC) are applied along x and y-axis, while perfectly matched layers (PMLs) are placed in the z-direction. A plane wave source propagating in the z-direction with a wavelength range span from 400 to 1100 nm is placed on the top of the structure as can be seen in the Fig. 1. To measure the exact transmittance a transmittance monitor is positioned at the interface of Si substrate and the NSs, while a reflectance monitor is positioned behind the source to measure the reflectance from the device structure. To record the electric field profile, scattering cross-section, absorption, photogeneration, and photocurrent, four distinct monitors are used, as illustrated in Fig. 1. To reduce computational load and save time, the lower limit for all these monitors is set at 500 nm into the Si substrate. Therefore, the Si thickness considered here is only 500 nm. To enhance the numerical accuracy of the program a finer mesh of size 2 nm is used for the NSs and for the rest of the FDTD region a non-uniform meshing is applied. The refractive index of the Si, Al, Ag, Au, and Cu are sourced from the internal data base of the Lumerical. The device structure for all four designed devices (Device-A, B, C, D) will remain consistent throughout the study, with the only variation being the material used for the nanospheres (NSs: Al, Ag, Au, and Cu for Device-A, B, C, and D, respectively).

RESULT AND DISCUSSION

Initially, we have set the period (p) at 400 nm and varied the radius (r) within the range of 10 to 150 nm for all the considered devices. To assess the performance of these devices, we compare them with a planar structure, i.e., a Si PV cell without NSs. The optimised value of r is determined for each device through an examination of various factors, including the reflectance, transmittance, NSs absorbance, device absorption, and solar generation rate. Subsequently, using the obtained optimised value of r, the value of p is varied from 250 to 650 nm. The same procedure is followed to obtain the optimised value of p as the one we have followed for the optimisation of the radius. Finally, a comparison is made between the performances of all the devices at their respective optimised values of r and p. The detailed discussion on the results is provided in the subsequent sections.

Effect of Radius Variation

When varying the radius of the NSs, we examined the average reflectance and transmittance for device-A as shown in Fig. 2(a) and (b). Notably, a significant lower average reflectance, particularly within the range of r_{Al} (radius of Al NS) from 60 to 140 nm, is observed. Therefore, to examine the spectral reflectance response over a range of wavelengths from 400 to 1100 nm, we have plotted it only within these ranges of r_{Al}. The reflectance spectrum, depicted in Fig. 2(c), exhibits a broad reduction in reflectance, primarily occurring within the 600 to 900 nm range when r_{Al} is set to 100 nm. This reduction in reflectance primarily occurs within the 600 to 900 nm range when r_{Al} is set to 100 nm. The decrease in reflectance can be attributed to the scattering effect of the Al NSs, which scatters the incident light to a wider range of angles, resulting in a longer path length for the light within the material and thus a higher probability of absorption. Fig. 2(d) illustrates that the best transmission of incident light into the Si substrate is also achieved at the same value of r_{Al}, which is 100 nm. This reduced reflectance and increased transmittance couples the maximum incident light power to the Si substrate, where it is absorbed to generate photocarriers. The absorption within the device is also examined and presented in Fig. 3(a). It has been observed that as the radius varies from 60 nm onwards, the absorbed power (P_{abs}) increases for the wavelength range from 650 to 1100 nm. The power loss, which is the power absorbed by the nanospheres (NSs), also increases as the radius increases beyond 100 nm. P_{abs} reduces significantly in the shorter wavelength region, as seen in Fig. 3(a) beyond 100 nm. The optimal value of r_{Al} is thus determined to be 100 nm, enhancing power absorption within the Si due to forward scattering and the plasmonic effect of the Al NSs, consequently leading to a higher generation rate and current density.

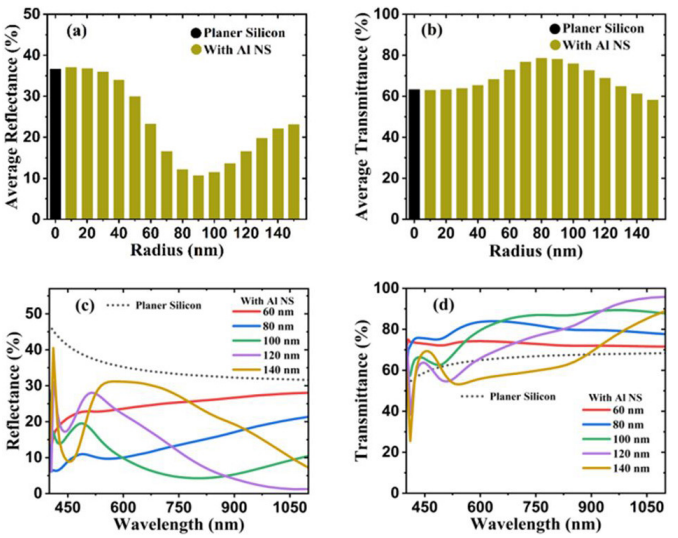

Fig. 2. The effect of the Al NS radius variation on (a) average reflectance, (b) average transmittance, (c) reflection spectrum, and (d) transmittance spectrum

Similarly, the average reflectance and transmittance for device-B are influenced by varying the radius (r_{Ag}) of Ag NSs. At a radius of 80 nm, the average reflectance reaches its minimum, while the average transmittance achieves its maximum. However, the maximum generation rate is observed at 60 nm of r_{Ag} due to enhanced light coupling into the semiconductor from the plasmonic resonance of Ag NS. The P_{abs} is particularly pronounced in the shorter wavelength range of 400 to 450 nm at r_{Ag} of 60 nm as can be seen in Fig. 3(b). Therefore, the optimised value for r_{Ag} is determined to be 60 nm.

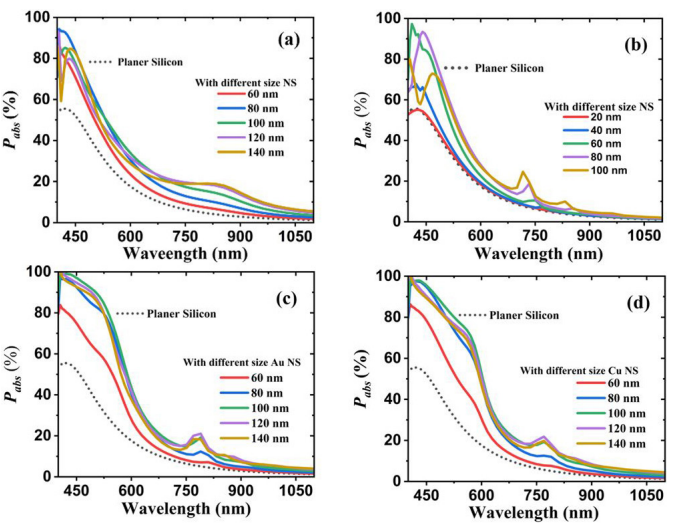

Fig. 3. Power absorption (P_{abs}) within the Si substrate at different radius of (a) Al nanosphere, (b) Ag nanosphere, (c) Au nanosphere, and (d) Cu nanosphere

For device-C with Au nanospheres, the minimum average reflectance occurs at r_{Au} (radius of Au NSs) of 100 nm, while the average transmittance remains nearly constant up to 80 nm for r_{Au} and decreases with further increases in r_{Au}. The decrease in average transmittance occurs due to spectral decrease in transmittance in shorter wavelengths, becoming more pronounced for r_{Au} beyond 80 nm. The absorbed power is maximised throughout the entire spectral range at r_{Au} of 100 nm, as shown in Fig. 3(c), leading to optimisation of r_{Au}

at 100 nm. On the other hand, for device-D with Cu NSs, the minimum average reflectance is achieved at r_{Cu} (radius of Cu NSs) of 100 nm, and the spectral reflectance response is particularly favorable at this radius compared to other spectral responses obtained with different r_{Cu} values. However, transmittance exhibits a decrease at shorter wavelengths as r_{Cu} increases, becoming more pronounced beyond 100 nm. The P_{abs} maximised throughout the entire spectral range at r_{Cu} of 100 nm, as depicted in Fig. 3(d), leading to optimised of r_{Cu} at 100 nm.

Effect of Periodicity

The period is systematically varied within the range of 250 to 650 nm for all devices, while keeping the radius of the NSs fixed at their respective optimised values.

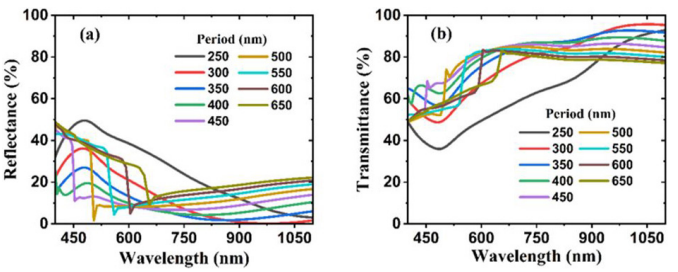

Fig. 4. Effect of Al NS period variation on (a) reflectance spectrum, and (b) transmittance spectrum

The reflectance and transmittance spectra of Device-A with Al NS are examined as shown in Fig. 4(a) and (b), respectively. The results reveal that the reflectance is at its minimum across the entire spectral range at a period (p_{AL}) of 400 nm, while the transmittance is maximised for this particular period value. The power loss, absorbed by the Al NS, at a period of 400 nm is relatively high for shorter wavelength ranges, specifically within the 400 to 450 nm range. However, beyond this range, this power loss significantly diminishes. While it is possible to further reduce this power loss by increasing the period beyond 400 nm, P_{abs} within the Si also decreases with an increase in period beyond 400 nm, as shown in Fig. 5(a). The most favorable spectral response for P_{abs} is achieved at 400 nm. Consequently, the value of p_{AL} is optimised at 400 nm, allowing for the simultaneous attainment of minimum reflectance, maximum transmittance, and maximum P_{abs}. Likewise, for Device-B with Ag NS, the period (p_{Ag}) is systematically varied. It is observed that as p_{Ag} increases from 250 nm and onwards, the spectral reflectance of the device also increases, while the transmittance reduces. However, the power loss in the NSs and P_{abs} within the silicon decrease when p_{Ag} is increased. It can be observed from Fig. 5(b) that at a p_{Ag} value of 300 nm, the P_{abs} is maximised only for very short wavelengths and remains nearly the same as that for the P_{abs} value of 250 nm across the rest of the spectral range. Therefore, 300 nm is considered as the optimised value for P_{abs} in this case.

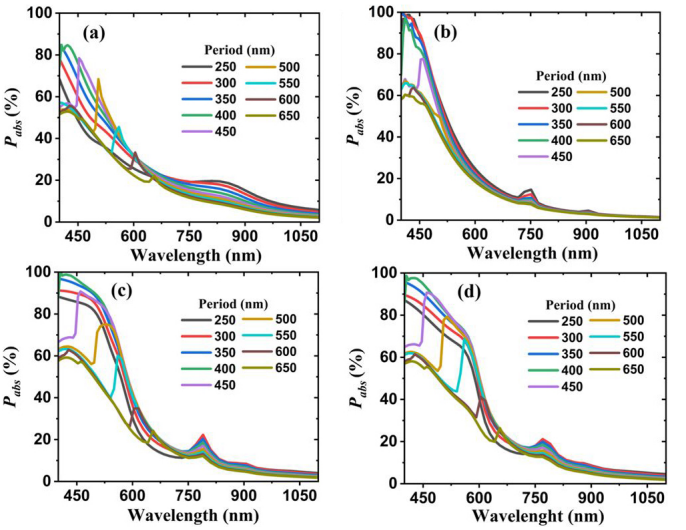

Fig. 5. Power absorption (P_{abs}) within the Si substrate at different period of (a) Al nanosphere, (b) Ag nanosphere, (c) Au nanosphere, and (d) Cu nanosphere

For device-C, the most favorable spectral responses for reflectance, transmittance, and P_{abs} within the Si are all achieved at a period (p_{Au}) of 400 nm, as evident from Fig. 5(c). A similar behavior of power loss (power absorption within the Au NS) is noticed, as in the previous case. It can be minimised by increasing the value of p_{Au} beyond 400 nm, but this comes at the cost of reduced P_{abs}, see Fig. 5(c). Therefore, the optimised choice for p_{Au} is determined to be 400 nm for Device-C. Finally, for device-D, the optimal spectral response in terms of reflectance, transmittance, and P_{abs} is achieved at a period (p_{Cu}) of 400 nm, as illustrated in Fig. 5(d). Consequently, the optimised choice for p_{Cu} is considered at 400 nm.

Performance Comparison of All the Devices

A comparison is made between the performances of all the devices at their respective optimised values of r and p. The transmittance and the power absorbed within the silicon (P_{abs}) for the all the devices are compared at their respective optimised values of radius and period, and these comparisons are presented in Fig. 6.

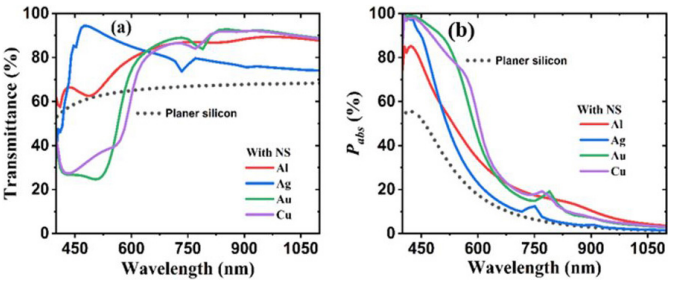

Fig. 6. Comparison of (a) transmittance spectrum, and (b) absorbance of the device at the respective optimised values of radius and period

The results reveals that in the shorter wavelength region below 650 nm, the transmittance is relatively higher for the devices-A and B, with the maximum transmittance observed in the device consisting Ag NS. However, in the wavelength range from 650 to 1100 nm, the devices-A, C and D exhibit higher transmittance, with maximum values that are nearly the same for the devices-C and D, i.e. the devices with Au and Cu NSs. Consequently, the best spectral distribution of the absorbed power (P_{abs}) is also obtained for the devices with Au and Cu NSs, as illustrated in Fig. 6(b). This relatively higher P_{abs} for the devices with Au and Cu NSs can be primarily attributed to the comparatively enhanced plasmonic effect of these metal nanoparticles. This enhancement is evident from the electric field distribution at a wavelength of 500 nm for all the devices, as shown in Fig. 7.

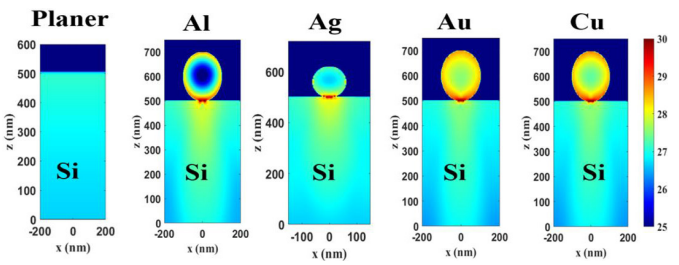

Fig. 7. Electric filed distribution for the planner and the devices with NSs at the wavelength of 500 nm

Finally, the short-circuit current density (J_{SC}) is computed for all these devices and compared with the J_{SC} of the planar device. The comparison is presented in Table 1. It has been observed that the device-D i.e., the device consisting Cu NSs with obtained optimum radius (r_{Cu}) of 100 nm and a period (p_{Cu}) of 400 nm yields the highest enhancement in the J_{SC} value. The result of the best device, i.e. the device-D is also been compared with the previously reported values of J_{SC} in the literature and are presented in Table 2.

Table 1. Comparison table of current densities

S. No.	*Device*	*J_{SC} (mA/cm²)*	*Relative Increase in J_{SC} (%)*
1	Planer	5.79	-
2	Device-A	10.95	89.12
3	Device-B	9.08	56.82
4	Device-C	13.46	132.46
5	Device-D	13.88	139.72

Table 2. Comparison of the results with reported literature

S. No.	*J_{SC} (mA/cm²)*	*Reference*
1	21.00	[28]
2	27.73	[17]
3	31.40	[29]
5	139.72	Our results

CONCLUSION

The study demonstrates that substantial enhancement of optical absorption in thin-film silicon is achievable by strategically arranging metal nanoparticles (NPs) directly on its top. Notably, the investigation identifies gold (Au) and copper (Cu) NPs as the most effective at inducing a strong plasmonic effect, with Cu exhibiting the maximum enhancement in silicon. Furthermore, the incorporation of NPs on the silicon surface significantly reduces surface reflectance due to the forward scattering of NPs. This dual impact of plasmonic enhancement and reduced reflectance leads to a remarkable improvement in current density, increasing it from 5.79 mA/cm² to 10.95 mA/cm², 90.8 mA/cm², mA/cm², and 13.88 mA/cm² for devices featuring Al, Ag, Au, and Cu NPs, respectively.

ACKNOWLEDGMENT

Mr. Mohd Amir hereby expresses his gratitude to Maulana Azad National Fellowship (MANF), SRF for the financial assistance. We are especially thankful to Ansys for providing a trial version of Lumerical FDTD.

REFERENCES

[1] C. D. Geddes, "Plasmonics - A vision for the future," *Plasmonics*, vol. 1, no. 1, pp. 1–2, Mar. 2006, doi: 10.1007/S11468-006-9010-Y/METRICS.

[2] S.A. Maier, "Plasmonics: Fundamentals and applications," *Plasmon. Fundam. Appl.*, pp. 1–223, 2007, doi: 10.1007/0-387-37825-1/COVER.

[3] X. Ren et al., "High Efficiency Organic Solar Cells Achieved by the Simultaneous Plasmon-Optical and

Plasmon-Electrical Effects from Plasmonic Asymmetric Modes of Gold Nanostars," *Small*, vol. 12, no. 37, pp. 5200–5207, Oct. 2016, doi: 10.1002/SMLL.201601949.

[4] R. Bhatia and L. Kumar, "Functionalized carbon nanotube doping of P3HT:PCBM photovoltaic devices for enhancing short circuit current and efficiency," *J. Saudi Chem. Soc*., vol. 21, no. 3, pp. 366–376, Mar. 2017, doi: 10.1016/J.JSCS.2016.11.003.

[5] P. Mandal, "Application of Plasmonics in Solar Cell Efficiency Improvement: a Brief Review on Recent Progress," *Plasmon*. *2022*, vol. 17, no. 3, pp. 1247–1267, Mar. 2022, doi: 10.1007/S11468-022-01616-9.

[6] B. Gallinet, J. Butet, and O. J. F. Martin, "Numerical methods for nanophotonics: Standard problems and future challenges," *Laser Photon. Rev*., vol. 9, no. 6, pp. 577–603, Nov. 2015, doi: 10.1002/LPOR.201500122.

[7] Y. A. Akimov and W. S. Koh, "Design of Plasmonic Nanoparticles for Efficient Subwavelength Light Trapping in Thin-Film Solar Cells," *Plasmonics*, vol. 6, no. 1, pp. 155–161, Mar. 2011, doi: 10.1007/S11468-010-9181-4/FIGURES/10.

[8] A. Said, K.S.R. Atia, and S.S.A. Obayya, "On modeling of plasmonic devices: overview," *JOSA B*, Vol. 37, Issue 11, pp. A163-A174, vol. 37, no. 11, pp. A163–A174, Nov. 2020, doi: 10.1364/JOSAB.399121.

[9] D. Sharma, R. K. Sharma, A. Srivastava, P. Kumari, and S. K. Srivastava, "Simulation Study on Broadband Light Harvesting Properties of Aluminium Nanosphere and Silicon Nanopillar Arrays based Tandem Structure," *Silicon*, vol. 15, no. 3, pp. 1211–1220, Feb. 2023, doi: 10.1007/S12633-022-02100-Z/METRICS.

[10] P. Banerjee et al., "Light-trapping scheme using silica spheres on ultrathin c-silicon absorber: Transition from antireflection coating to whispering gallery resonator," *Appl. Phys. A Mater. Sci. Process*., vol. 128, no. 6, pp. 1–11, Jun. 2022, doi: 10.1007/S00339-022-05591-0/FIGURES/13.

[11] P. Kou, L. Yang, C. Chang, and S. He, "Improved Flexible Transparent Conductive Electrodes based on Silver Nanowire Networks by a Simple Sunlight Illumination Approach," *Sci. Reports 2017*, vol. 7, no. 1, pp. 1–11, Feb. 2017, doi: 10.1038/srep42052.

[12] M. Yao et al., "Performance Improvement of Polymer Solar Cells by Surface-Energy-Induced Dual Plasmon Resonance," *ACS Appl. Mater. Interfaces*, vol. 8, no. 9, pp. 6183–6189, Mar. 2016, doi: 10.1021/ACSAMI.6B00297.

[13] W.A. Murray and W.L. Barnes, "Plasmonic Materials," *Adv. Mater*., vol. 19, no. 22, pp. 3771–3782, Nov. 2007, doi: 10.1002/ADMA.200700678.

[14] P.E. Batson, "Plasmonic Modes Revealed," *Science* (80), pp. 333–334, Jan. 2012, doi: 10.1126/SCIENCE.1215588.

[15] D. Sharma, R.K. Sharma, A. Srivastava, P. Kumari, and S.K. Srivastava, "Simulation Study on Broadband Light Harvesting Properties of Aluminium Nanosphere and Silicon Nanopillar Arrays based Tandem Structure," *Silicon*, vol. 15, no. 3, pp. 1211–1220, Feb. 2023, doi: 10.1007/S12633-022-02100-Z/METRICS.

[16] P. Spinelli et al., "Plasmonic light trapping in thin-film Si solar cells," *J. Opt*., vol. 14, no. 2, p. 024002, Jan. 2012, doi: 10.1088/2040-8978/14/2/024002.

[17] S. Foroutan, G. Rostami, M. Dolatyari, and A. Rostami, "Improvement of the conversion efficiency and power of thin film silicon solar cells by embedding metallic nanostructures in depletion region," *Optik* (*Stuttg*)., vol. 127, no. 20, pp. 8988–8994, Oct. 2016, doi: 10.1016/J.IJLEO.2016.06.100.

[18] H. A. Atwater and A. Polman, "Plasmonics for improved photovoltaic devices," *Nat. Mater*. 2010 93, vol. 9, no. 3, pp. 205–213, Feb. 2010, doi: 10.1038/nmat2629.

[19] P. Spinelli, M. Hebbink, R. De Waele, L. Black, F. Lenzmann, and A. Polman, "Optical impedance matching using coupled plasmonic nanoparticle arrays," *Nano Lett*., vol. 11, no. 4, pp. 1760–1765, Apr. 2011, doi: 10.1021/NL200321U.

[20] K. Zhou, S. W. Jee, Z. Guo, S. Liu, and J. H. Lee, "Enhanced absorptive characteristics of metal nanoparticle-coated silicon nanowires for solar cell applications," *Appl. Opt*., vol. 50, no. 31, Nov. 2011, doi: 10.1364/AO.50.000G63.

[21] O. Pylypova et al., "Influence of nanostructure geometry on light trapping in solar cells," *Appl. Nanosci*., vol. 12, no. 3, pp. 769–774, Mar. 2022, doi: 10.1007/S13204-021-01699-6/METRICS.

[22] H. Li et al., "Which method is more efficient on enhancing light absorption for silicon nanowires array based solar cells: Plasmonic metal nanoparticles or narrow-bandgap semiconductor quantum dots?," *Mater. Sci. Semicond. Process*., vol. 146, p. 106661, Aug. 2022, doi: 10.1016/J.MSSP.2022.106661.

[23] P.R. Pudasaini and A.A. Ayon, "Modeling the front side plasmonics effect in nanotextured silicon surface for thin film solar cells application," *Microsyst. Technol*., vol. 19, no. 6, pp. 871–877, Jun. 2013, doi: 10.1007/S00542-013-1756-5/FIGURES/6.

[24] X. Huang, C. Lou, H. Zhang, and H. Yang, "Broadband anti-reflection in Si substrate via Ag nanospheres on Si nanopillar arrays," *Opt. Commun*., vol. 460, p. 125133, Apr. 2020, doi: 10.1016/J.OPTCOM.2019.125133.

[25] K. R. Catchpole and A. Polman, "Design principles for particle plasmon enhanced solar cells," *Appl. Phys. Lett*., vol. 93, no. 19, p. 191113, Nov. 2008, doi: 10.1063/1.3021072/335818.

[26] K. S. Yee and J.S. Chen, "The finite-difference time-domain (FDTD) and the finite-volume time-domain

(FVTD) methods in solving Maxwell's equations," *IEEE Trans. Antennas Propag.*, vol. 45, no. 3, pp. 354–363, 1997, doi: 10.1109/8.558651.

[27] S.D. Gedney, "Introduction to the Finite-Difference Time-Domain (FDTD) Method for Electromagnetics," *Introd. to Finite-Difference Time-Domain Method Electromagn.*, 2011, doi: 10.1007/978-3-031-01712-4.

[28] H. Li, Y. Hu, Y. Yang, and Y. Zhu, "Theoretical investigation of broadband absorption enhancement in a-Si thin-film solar cell with nanoparticles," *Sol. Energy Mater. Sol. Cells*, vol. 211, p. 110529, Jul. 2020, doi: 10.1016/J.SOLMAT.2020.110529.

[29] D. Sharma, P. Kumari, A. Srivastava, and S.K. Srivastava, "Comparative Numerical Analysis of Broadband Light Trapping Structures Based on Plasmonic Metals Nanosphere and Silicon Nanopillar Arrays for Thin Solar Cells," *Plasmonics*, vol. 18, no. 2, pp. 701–710, Apr. 2023, doi: 10.1007/S11468-023-01796-Y/TABLES/2.